








# InP-Based THz Beam Steering Leaky-Wave Antenna

Peng Lu , Thomas Haddad , *Graduate Student Member, IEEE*, Benedikt Sievert , Beshar Khani , Sumer Makhlof , Sebastian Dülme , José Fernández Estévez, Andreas Rennings , *Member, IEEE*, Daniel Erni , *Member, IEEE*, Ullrich Pfeiffer , *Fellow, IEEE*, and Andreas Stöhr, *Senior Member, IEEE*

**Abstract**—For mobile THz applications, integrated beam steering THz transmitters are essential. Beam steering approaches using leaky-wave antennas (LWAs) are attractive in that regard since they do not require complex feeding control circuits and beam steering is simply accomplished by sweeping the operating frequency. To date, only a few THz LWAs have been reported. These LWAs are based on polymer or graphene substrates and thus, it is quite impossible to monolithically integrate these antennas with state-of-the-art indium phosphide (InP)-based photonic or electronic THz sources and receivers. Therefore, in this article, we report on an InP-based THz LWA for the first time. The developed and fabricated THz LWA consists of a periodic leaking microstrip line integrated with a grounded coplanar waveguide to microstrip line (GCPW-MSL) transition for future integration with InP-based photodiodes. For fabrication, a substrate-transfer process using silicon as carrier substrate for a 50- $\mu\text{m}$  thin InP THz antenna chip has been established. By changing the operating frequency from 230 to 330 GHz, the fabricated antenna allows to sweep the beam direction quasi-linearly from  $-46^\circ$  to  $42^\circ$ , i.e., the total scanning angle is  $88^\circ$ . The measured average realized gain and 3-dB beam width of a 1.5-mm wide InP LWA are  $\sim 11$  dBi and  $10^\circ$ . This article furthermore discusses the use of the fabricated LWA for THz interconnects.

**Index Terms**—Beam steering, indium phosphide (InP), leaky-wave antenna (LWA), monolithic integrated circuits, wafer bonding.

## I. INTRODUCTION

**T**ERAHERTZ (THz) waves feature distinct advantages compared to its neighboring spectra, making this frequency spectrum (0.1–10 THz) very attractive for several applications.

Manuscript received July 11, 2020; revised September 23, 2020; accepted October 26, 2020. Date of publication November 19, 2020; date of current version March 3, 2021. This work was supported by the Deutsche Forschungsgemeinschaft (DFG, German Research Foundation) under Project-ID 287022738 – TRR 196. (Corresponding author: Peng Lu.)

Peng Lu, Thomas Haddad, Sumer Makhlof, Sebastian Dülme, José Fernández Estévez, and Andreas Stöhr are with the Department of Optoelectronics, University of Duisburg-Essen, 47057 Duisburg, Germany (e-mail: peng.lu@uni-due.de; thomas.haddad@uni-due.de; sumer.makhlof@uni-due.de; sebastian.duelme@uni-due.de; jose.fernandez-estevez@uni-due.de; andreas.stoehr@uni-due.de).

Beshar Khani is with the NTT Germany AG & Co. KG, 61352 Bad Homburg vor der Höhe, Germany (e-mail: beshar.khani@uni-due.de).

Benedikt Sievert, Andreas Rennings, and Daniel Erni are with the Department of General and Theoretical Electrical Engineering, University of Duisburg-Essen, 47057 Duisburg, Germany (e-mail: benedikt.sievert@uni-due.de; andre.rennings@uni-due.de; daniel.erni@uni-due.de).

Ullrich Pfeiffer is with the Institute for High-frequency and Communication Technology, University of Wuppertal, 42119 Wuppertal, Germany (e-mail: ullrich.pfeiffer@uni-wuppertal.de).

Color versions of one or more of the figures in this article are available online at doi.org/10.1109/TTHZ.2020.3039460.

Digital Object Identifier 10.1109/TTHZ.2020.3039460

THz waves are far less energetic than X-rays, i.e., they are nonionizing for biological tissues and, consequently, are promising for several medical applications [1]–[4]. Benefiting from the shorter wavelength in contrast to microwaves, THz waves offer a much higher spatial resolution, which makes them quite intriguing for high-resolution imaging applications [5], [6]. Beyond the high spatial resolution, most dry dielectric materials are transparent for THz waves, whereas materials with high electrical conductivity or with large static dipoles (i.e., metals and water) are strong reflectors or absorbers for THz waves. This leads to high image contrasts [7], [8]. In addition, THz spectroscopy systems have received much attention, benefiting from the unique fingerprint spectra of various chemical compounds [9], [10]. Not the least, in comparison to the scarce available spectrum in the microwave region, THz waves offer a much wider available bandwidth which is crucial for future high data-rate wireless communications [11]–[13] and short-range THz interconnects [14]. Reconfigurable short-range high data rate THz interconnects would be very beneficial, e.g., for data centers and even for intramachine communications.

The above-mentioned applications have stimulated technological advances mainly focusing on the development of THz sources and THz receivers with higher transmit power levels and better sensitivities [15]–[17]. However, despite the fact that there have been great achievements in that regard, high-gain THz antennas and THz beam steering technologies are still essential for many applications, such as THz interconnects, to overcome the comparably high THz free-space path loss (FSPL). This is on the one hand to relax requirements of the employed THz transmitter and THz receiver but moreover to enable mobility and spatial multiplexing.

In the recent past, different THz beam steering approaches have been investigated, including, for instance, microelectromechanical systems (MEMS) enhancing the scanning-speed and precision compared to classical mechanical approaches [18]. Also, several electronic approaches such as phased-array transmitter [19], electronically controlled metasurfaces based on  $\text{VO}_2$  [20], or graphene reflect arrays [21] have been studied. Also, photonic beam steering approaches have attracted much attention. This is because photonics offers some key generic advantages with respect to beam steering, which include a wide operational bandwidth, the availability of low phase noise sources, and a compact chip size [22], [23]. Furthermore, it is possible to transfer phase shifts and even true time delays performed in the infrared domain to the THz regime for beam steering. By means of an  $1 \times 4$  photomixer array and fiber-optic

delay lines, 1-D beam steering within an angle of  $35^\circ$  at 600 GHz has been realized [24]. In [25], the THz beam has been steered with a maximum angle of  $29^\circ$  by using an array of photoconductive antennas (PCAs) and a free-space optical phase shifter approach. However, the complex optical phase shifters required in both cases prevent monolithic photonic integration.

Leaky-wave antennas (LWAs) do not require such complex phase shifter or true time delay feeders since here, beam steering is achieved by tuning the carrier frequency [26]. Thus, THz LWAs are envisaged to be an attractive solution for applications such as THz interconnects which necessitate robust and highly integrated THz beam steering antennas. This in turn requires that the THz LWA can be integrated with state-of-the-art photonic or electronic sources and receivers.

In previous works, some first THz LWAs have already been realized. In [27], a THz LWA based upon a metamaterial waveguide with a quantum cascade laser (QCL) is reported. A microstrip periodic LWA based on polymer substrate fed by a vector network analyzer (VNA) is shown in [28]. The disadvantage of these approaches is that the developed LWAs could not be monolithically integrated with state-of-the-art chip-sized photonic or electronic THz sources and receivers, which are typically based upon indium phosphide (InP) substrate. For photonics, this is to enable the use of mature  $1.55\ \mu\text{m}$  IR laser diodes, modulators, and amplifiers and for electronics, this is because InP transistors offer the highest maximum oscillation frequencies and transit frequencies [29], [30]. For 26 GHz 5G band and E band, several LWAs based upon low-permittivity substrates have been hybrid integrated with InP photodiodes using wire bonding [31]–[33]. However, at THz frequencies, wire bonding will lead to high losses [34], [35]. Therefore, we here propose the use of THz LWAs based upon InP substrate for future monolithic and low-loss integration with THz photodiodes.

In this work, we report on an InP-based THz beam steering LWA. The design of the fabricated InP THz LWA studied in this work is motivated by future integration with InP THz photodiodes to realize monolithically integrated robust beam steering THz transmitter chips. To our knowledge, this is the first InP-based THz beam steering LWA. The target applications we focus at are short-range THz communications, i.e., THz interconnects and THz image scanner. For THz interconnects, the targets are to achieve an antenna realized gain and a coherence bandwidth of at least 10 dBi and 10 GHz, respectively. Given the output power of THz photodiodes which is about  $-20\ \text{dBm}$  at 300 GHz and considering further the free-space path loss, atmospheric attenuation, THz envelope receiver sensitivity, and required SNR, such antennas are expected to support data rates of at least 10 Gb/s over 30 cm using QPSK modulation [13]. The maximum beam steering angle is mainly defined by the permittivity of the antenna's substrate [36]. For InP, a scanning angle around  $90^\circ$  for a full-band WR3 band THz LWA antenna is expected. This will be further discussed in Section III.

In detail, we report on a microstrip-type InP LWA for the 0.3-THz WR3 waveguide band. The THz LWA is designed using CST Studio Suite. To enable future integration with triple-transit-region photodiodes (TTR-PDs), the LWA features a grounded coplanar waveguide to microstrip line (GCPW-MSL)

THz transition whose design is also novel to our knowledge. To reduce the number of surface wave modes and thus, increase the radiation efficiency of the THz LWA, a silicon (Si) substrate-transfer process has been developed to enable fabrication of the THz LWA on a  $50\text{-}\mu\text{m}$  thin grounded InP substrate. We also created an on-wafer antenna measurement system for characterizing the radiated THz beam in the far-field.

The manuscript is organized as follows. In Section II, the motivation for developing integrated InP-based photonic THz beam steering transmitter chips is discussed. Section III reports on the designs of the InP THz LWA and the InP GCPW-MSL THz transition. The developed substrate-transfer fabrication process is described in Section IV. Section V presents the experimentally determined THz scattering parameters, the measured THz beam profiles, and the THz scanning angles. The experimental findings are also compared with the simulated performances. Finally, in Section VI, we discuss the potential of using the developed LWA for THz interconnects.

## II. CONCEPT OF A PHOTONIC INTEGRATED THz TRANSMITTER

As mentioned above, first THz LWAs were demonstrated in [27] and [28]. However, these approaches required liquid-nitrogen cooling or used bulky VNAs with THz extenders as signal sources. An InP-based THz LWA is quite attractive because it would enable monolithic integration with InP-based THz photodiodes and room temperature operation. Today, THz photodiodes offer reasonably high output power, typically reaching several  $10\ \mu\text{W}$  @ 0.3 THz [37], [38]. This opens the potential for a photonic integrated circuit (PIC) consisting of an InP-based photodiode monolithically integrated with a THz LWA to create a THz beam steering transmitter chip. Even monolithic integration of  $1.55\ \mu\text{m}$  laser diodes can be envisaged.

The high permittivity and low loss tangent of InP contribute to reducing the overall antenna dimensions and losses in the InP substrate [39], [40]. In addition, the higher permittivity of InP as compared to low-permittivity substrates such as polymers, leads to a smaller period of LWA unit cells, which results in an increase of the beam-scanning angle [36].

When using InP as substrate material for the antenna, the substrate thickness becomes one of the most crucial design parameters as it defines the number of surface wave modes in the substrate which have a strong impact on the LWA performance [41]. A thick substrate would lead to more bounded surface wave modes which cannot be radiated along the LWA and thus, cause a degradation of the radiation efficiency [42]. Here, a  $50\text{-}\mu\text{m}$  thin InP substrate is used for antenna fabrication. This in turn necessitates the use of a mechanical carrier substrate.

A schematic view of the proposed photonic THz beam steering transmitter chip based upon the above considerations is illustrated in Fig. 1. A Si substrate is used as the carrier for the InP-based THz photodiode and LWA. An Au layer is utilized as bonding layer and functions as ground plane for the THz LWA. For fabrication, the InP substrate is bonded on the Si substrate using thermocompression bonding (TCB). Epitaxial layers of photodiodes will be grown on the grinded and polished InP substrate. After that, photodiodes and antennas will be

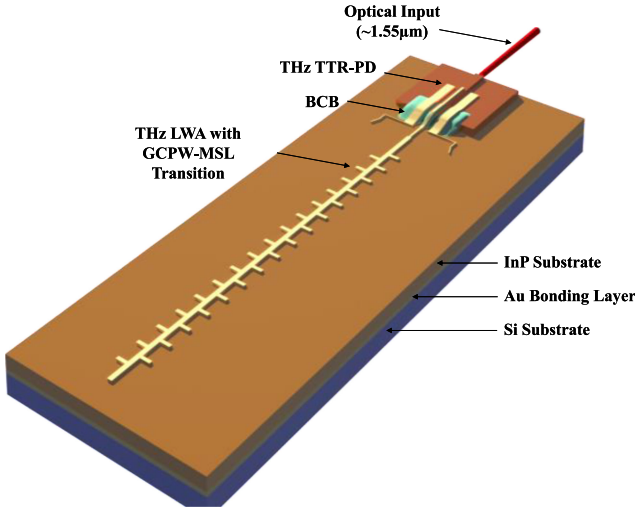


Fig. 1. Conceptual image of a THz microstrip periodic LWA with an on-chip integrated TTR-PD on an InP-to-Si bonded wafer.

fabricated using standard lithography technology. For connecting the photodiode with the LWA, a GCPW-MSL transition is required and BCB is used as a passivation layer to avoid short circuits between the p- and n-contacts of the PD (see also Fig. 1). BCB also functions as a planarization layer, helping to avoid breakage of the metallic signal and ground transmission lines.

### III. THZ LWA AND GCPW-MSL TRANSITION DESIGN

#### A. LWA Design

For the microwave frequency region, different LWA topologies have been studied, including rectangular waveguides [43], [44], substrate integrated waveguides (SIWs) [26], [45]–[47], or coplanar waveguides (CPWs) [48], [49]. However, for the THz frequency region, open guided-wave structures are preferred because of the lower transmission loss [50]. Microstrip LWAs featuring open guided-wave structures have been intensively investigated due to the simple fabrication process, lightweight, and better integration with active sources [28], [51], [52]. Therefore, we develop a THz LWA based on microstrip line in this work. To facilitate the integration with THz photodiodes that usually feature a GCPW output, an additional GCPW-MSL transition is needed. The resulting layout of the developed THz LWA with the integrated GCPW-MSL transition is shown in Fig. 2.

For future monolithic integration of the microstrip LWA with our InP-based 300 GHz TTR-PDs, the LWA's input impedance is designed to be similar to the impedance of the TTR-PDs, which is around  $35 \Omega$ . There are several models to mathematically analyze the input impedance of a microstrip [53]–[55]. In this work, we use the model described in [55], where the characteristic impedance  $Z_0$  is a function of microstrip width  $w$ , relative permittivity of InP substrate  $\epsilon_r$  ( $\epsilon_r \approx 12.4$  [40]), and substrate thickness  $h$  as defined in (1) and (2) in the following:

$$\frac{w}{h} = \frac{8e^A}{e^{2A} - 2} \text{ for } \frac{w}{h} < 2 \quad (1)$$

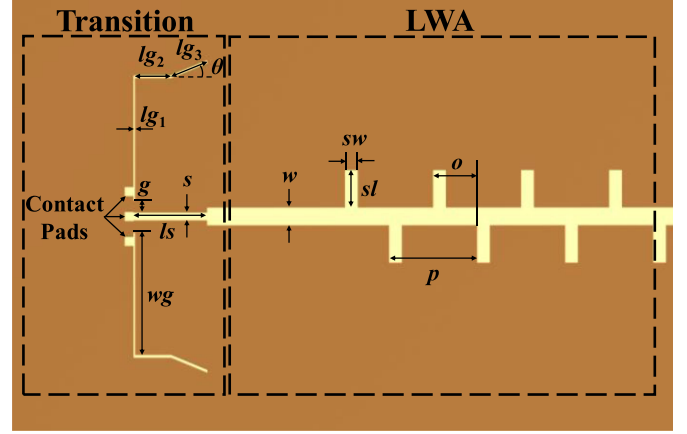


Fig. 2. Schematic top view of the microstrip periodic LWA with a GCPW-MSL transition on an InP-to-Si bonded wafer.

with the parameter  $A$

$$A = \frac{Z_0}{60} \sqrt{\frac{\epsilon_r + 1}{2} + \frac{\epsilon_r - 1}{\epsilon_r + 1} \left(0.23 + \frac{0.11}{\epsilon_r}\right)}. \quad (2)$$

Here,  $w/h$  is equal to 1.4691, i.e.,  $w/h < 2$ , and thus, according to the model, the width of the microstrip should be  $w = 73.46 \mu\text{m}$ . By computational electromagnetics simulations using CST Studio Suite, we finally found the optimum width to be  $w = 70 \mu\text{m}$ .

In a simple straight MSL, the quasi-TEM mode would not be radiated, because the phase constant  $\beta$  of the quasi-TEM mode is larger than the free-space wavenumber  $k_0$ . In other words, the dominant mode in a straight MSL is a slow wave. To make the dominant mode a fast wave, i.e., a mode that is radiated, we utilize 32 periodic rectangular stubs as comb-lines on both sides of the microstrip. This design creates an infinite number of space harmonics with the phase constants  $\beta_n$  [42]

$$\beta_n = \beta_0 + \frac{2n\pi}{p} \quad (3)$$

where  $p$  is the period and  $\beta_0$  is phase constant of the fundamental space harmonic. To achieve a single beam radiation, LWAs are designed to ensure a unitary fast space harmonic ( $n = -1$ ) [42]. The period  $p$  between stubs is equal to the guided wavelength  $\lambda_g$  [52], which can be calculated through [55]

$$\lambda_g = \frac{c_0}{f\sqrt{\epsilon_{\text{eff}}}} \quad (4)$$

where  $f$  is the operating frequency of the antennas. In this work, the LWA is designed for 230 to 330 GHz operation with a center frequency  $f = 280$  GHz. The effective permittivity of the microstrip line on the  $50\text{-}\mu\text{m}$  thick InP-substrate can be calculated using [55]

$$\epsilon_{\text{eff}} = \frac{\epsilon_r + 1}{2} + \frac{\epsilon_r - 1}{2\sqrt{1 + \frac{12h}{w}}} \text{ for } w/h > 1. \quad (5)$$

This results in an effective permittivity of  $\epsilon_{\text{eff}} = 8.56$ . Thus, according to the model and (5), the period should be  $p = 366 \mu\text{m}$ . By means of CST Studio Suite, we then found the



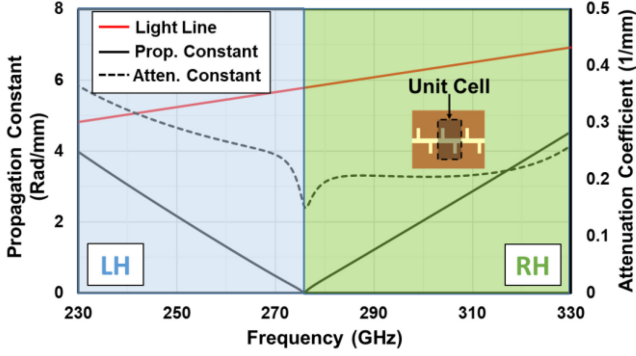


Fig. 3. Simulated dispersion diagram of a single LWA unit cell.

optimum period to be  $p = 353 \mu\text{m}$ , where the simulated effective permittivity of the antenna changes from 9.74 to 10.14 as the frequency varies from 230 to 330 GHz.

To determine the beam steering angle and the 3-dB beam width of the LWA, the simulated dispersion diagram is provided for a single unit cell. As can be observed from Fig. 3, the phase constant of the first space harmonic ( $n = -1$ ) is smaller than the free-space propagation constant (light line) from 230 to 330 GHz, i.e., a fast wave is generated and radiates from the LWA. In the left-handed (LH) region, the beam is steered toward backfire for decreasing frequency. In the right-handed (RH) region, the beam is steered toward endfire as the frequency increases. The beam direction from broadside is given by [42]

$$\sin \theta_m \approx \frac{\beta_{-1}}{k_0}. \quad (6)$$

Therefore, a beam steering range of  $\sim 95^\circ$  is expected from 230 to 330 GHz with  $\sim 0.95^\circ/\text{GHz}$ . To achieve a coherence bandwidth of 10 GHz for THz interconnects, the 3-dB beam width of LWA radiations at all frequencies must be larger than  $9.5^\circ$ , so that a fixed receiver can detect the spatially disperse THz signals. The 3-dB beam width of an infinite LWA can be calculated using [28]

$$\theta_w = \frac{2\alpha c_0}{2\pi f \cos \theta_{-1}} \quad (7)$$

where  $\alpha$  is the attenuation coefficient of an LWA and  $c_0$  is the speed of light in vacuum. As can be seen from Fig. 3, the minimum  $\alpha$  is  $\sim 0.15 \text{ mm}^{-1}$  at broadside with  $sl = 150 \mu\text{m}$  and  $sw = 50 \mu\text{m}$ . Therefore, a 3-dB beam width larger than  $10^\circ$  is expected even for broadside.

It is well known that for periodic LWAs, the open-stop band (OSB) effect causes a nonnegligible decrease of the antenna's gain of broadside radiation. This is caused by contradirectional coupling of space harmonics, which leads to a very high VSWR and a significantly suppressed radiation power in periodic LWAs with open structures [42], [56]. The presence of the OSB effect is represented on the attenuation curve in Fig. 3 as a small subsidence located at broadside. Fig. 4 shows the simulated Bloch impedance  $Z_B$  of the microstrip periodic LWA with 16 unit cells considering the mutual coupling and the edge effects. As can be seen in Fig. 4, a real, nonzero Bloch impedance

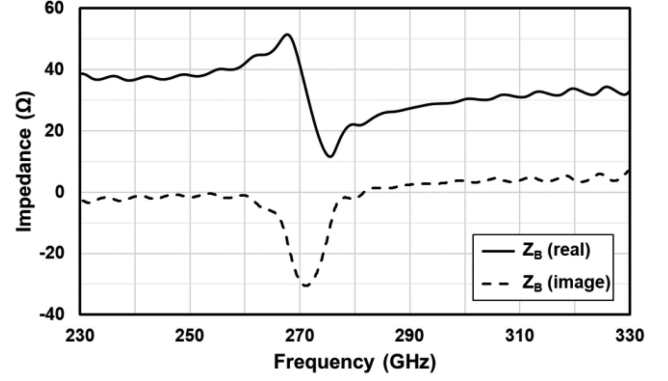


Fig. 4. Simulated Bloch impedance of the microstrip periodic LWA.

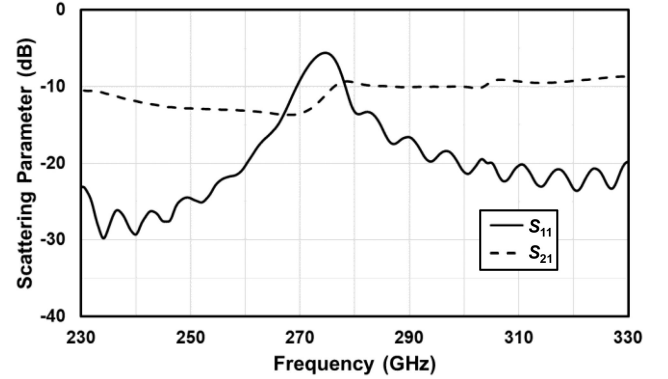


Fig. 5. Simulated scattering parameters of the microstrip periodic LWA.

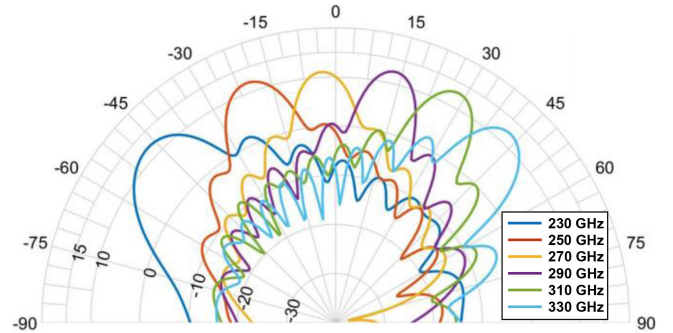


Fig. 6. Simulated far-field radiation patterns for the designed microstrip LWA at 230, 250, 270, 290, 310, and 330 GHz in the H-plane.

at broadside indicates that the OSB effect is mitigated at the broadside [57] with an accepted behavior regarding the chosen structure and the design target (realized gain larger than 10 dBi). For the further mitigation of the OSB effect, an asymmetric unit cell design could be used, as reported in [58].

As can be observed from Fig. 5, for most frequencies, the return loss is below 10 dB. At the broadside frequency, the return loss reaches a maximum of 5.6 dB. Nevertheless, as can be seen in Fig. 6, the maximum realized gain is about 12.5 dBi with a small penalty of about 2 dB for radiation at 270 GHz. The beam direction changes from backfire to endfire passing through

TABLE I  
PARAMETERS OF MICROSTRIP PERIODIC LWA

Symbol	Value	Description
$w$	70 $\mu\text{m}$	microstrip line width
$p$	353 $\mu\text{m}$	period
$sw$	50 $\mu\text{m}$	stub width
$sl$	150 $\mu\text{m}$	stub length
$o$	176.5 $\mu\text{m}$	stub offset

TABLE II  
COMPARISON OF GCPW-MSL TRANSITIONS

Freq. (GHz)	$S_{11}$ (dB)	$S_{21}$ (dB)	Substrate Material	Ref.
10-40	<-10	>-1	high-resistivity silicon	[59]
50-75	<-10	>-1.5	PET	[60]
DC-77	<-10	-0.2	BCB	[61]
75-110	<-18	-0.3	high-resistivity silicon	[62]
100-450	<-10	>-0.5	InP	This work

broadside. By increasing the frequency, the beam sweeps from  $-48^\circ$  at 230 GHz to  $43^\circ$  at 330 GHz with a minimum 3-dB beam width of  $\sim 10^\circ$ . Thus, the total beam steering angle is over  $91^\circ$  for a bandwidth of 100 GHz.

The overall radiation efficiency of the designed antenna, i.e., the ratio between the radiated power and the input power to the LWA used in CST for simulations, is around 60%, except for broadside where it is 51%.

All key parameters of the finally designed microstrip periodic LWA are summarized in Table I.

### B. GCPW-MSL Transition Design

For the microwave region, GCPW-MSL transitions can be realized as a surface-to-surface transition via electromagnetic coupling between ground conductors. As shown in Table II, several GCPW-MSL transitions have been demonstrated up to 110 GHz [59]–[62].

However, simulation results at THz frequencies reveal that the performance of such designs is far from optimum, because the excitation of parasitic substrate modes cannot be sufficiently suppressed by limiting the ground plane width of the GCPWs. This problem can be overcome by means of vertical interconnect access (VIA) holes [63]. However, the fabrication of deep VIAs in InP is not at all straightforward and substantially complicates the fabrication process. Therefore, we developed a novel GCPW-MSL transition that does not necessitate VIAs. The designed transition structure is shown in Fig. 2. Since the aim in this work is to experimentally characterize the LWA using a commercial WR-3 GSG-probe for proof-of-concept measurements, we considered a CPW pitch of 100  $\mu\text{m}$  at the beginning of the transition. The width of the signal line  $s$  was designed to be 30  $\mu\text{m}$  for impedance matching with the commercial GSG-probes. Instead of limited width ground planes, we designed short length ground planes to limit parasitic substrate modes.

The parameters of the GCPW-MSL transition are listed in Table III.

TABLE III  
PARAMETERS OF GCPW-MSL TRANSITION

Parameter	Value	Description
$s$	30 $\mu\text{m}$	Signal line width (GCPW)
$g$	50 $\mu\text{m}$	Gap (GCPW)
$ls$	295 $\mu\text{m}$	Signal line length (GCPW)
$wg$	500 $\mu\text{m}$	Ground-plate width
$lg_1$	5 $\mu\text{m}$	Ground-strip length 01
$lg_2$	150 $\mu\text{m}$	Ground-strip length 02
$lg_3$	157 $\mu\text{m}$	Ground-strip length 03
$\theta$	$22^\circ$	Angle of ground-strip 03

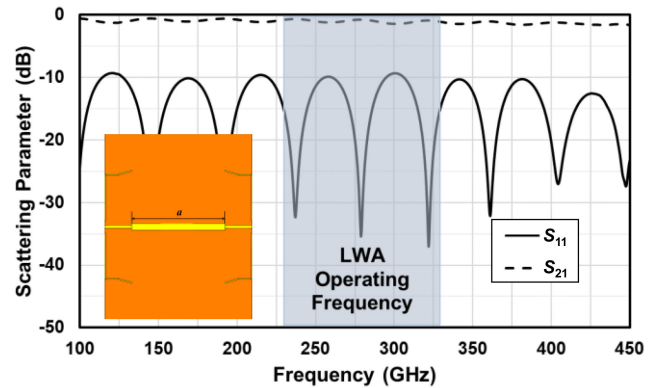


Fig. 7. Simulated scattering parameters of the back-to-back GCPW-MSL transition from 100 to 450 GHz. Inset shows the layout of the GCPW-MSL transition with a MSL length of  $a = 1$  mm.

Simulated scattering parameters of the back-to-back transition with a 1-mm long MSL ( $w = 70 \mu\text{m}$ ) are shown in Fig. 7. As can be observed, the designed transition yields a good matching over an extremely broad bandwidth which is crucial for the integration with an LWA. Simulation results show that  $S_{11}$  is lower than  $-10$  dB within a frequency range from 100 to 450 GHz. The periodic fluctuation is caused by the different signal pad widths of the transition and the MSL and can be optimized using a taper structure at the interface in the future. Furthermore, the insertion loss is reasonably small with a maximum loss below 1.6 dB over the entire frequency range and even below 1.4 dB for the operating frequency of the LWA. The simulated average loss of the 1000  $\mu\text{m}$  MSL is  $\sim 0.5$  dB, and therefore, the extracted insertion loss per transition is maximum 0.5 dB from 100 to 450 GHz.

### IV. FABRICATION

As discussed above, the development of InP-based beam steering LWAs requires  $\sim 50\text{-}\mu\text{m}$  thin InP layers. However, such thin InP substrates are extremely fragile and thus, difficult to be handled during the clean-room fabrication process. Therefore, we developed a substrate-transfer technology using a thick Si substrate to mechanically stabilize the thin InP substrate layer.

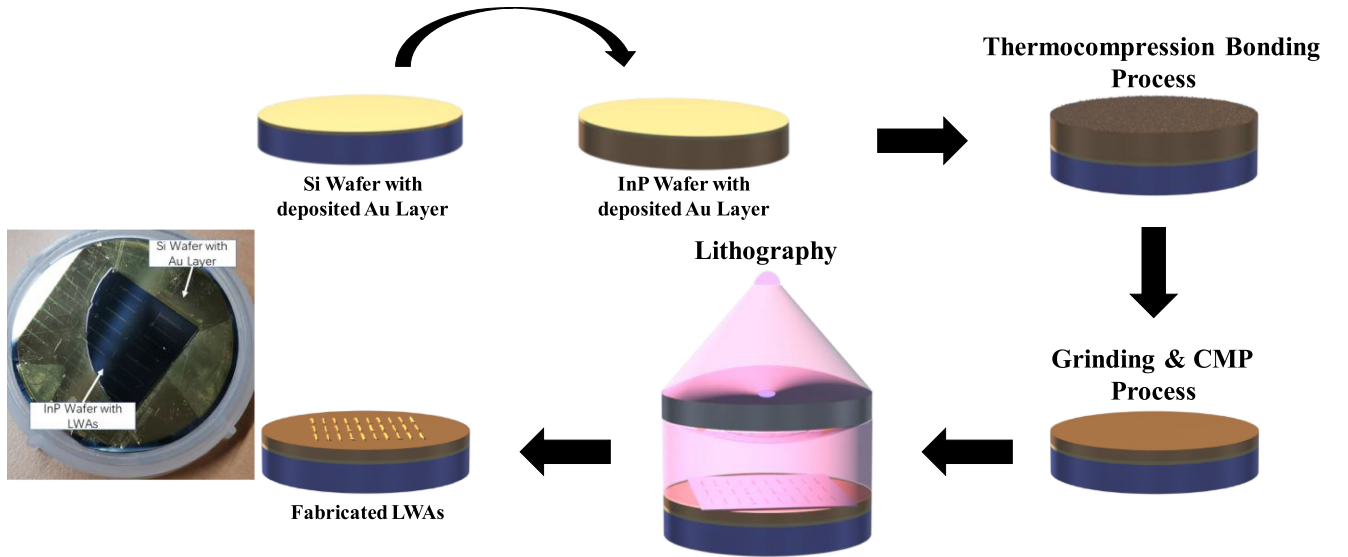


Fig. 8. Fabrication process flow of designed microstrip periodic LWAs with GCPW-MSL transitions based on substrate-transfer technology. The photograph shows the fabricated LWAs.

Fig. 8 sketches the entire fabrication process flow of the designed microstrip periodic LWA with the integrated GCPW-MSL transition. At first, 1- $\mu\text{m}$  thick Ti/Pt/Au layers were deposited on both sides, the surfaces of the InP and the Si substrate. Next, the InP and Si wafers were cleaned using acetone and isopropanol before TCB using a flip-chip bonder (SET FC150) with a bonding pressure of  $\sim 3$  MPa for about 4 h. Due to the mismatch of thermal expansion coefficients (TECs) between InP and Si ( $\alpha_{\text{InP}} = 4.8 \times 10^{-6} \text{ K}^{-1}$ ,  $\alpha_{\text{Si}} = 2.6 \times 10^{-6} \text{ K}^{-1}$ ) [64], the bonding temperature was limited to 250  $^{\circ}\text{C}$  in order to avoid mechanical stress between bonded wafers. The thickness of the InP substrate was reduced to 50  $\mu\text{m}$  by grinding followed by a chemical mechanical polishing (CMP) process to achieve a smooth surface, which is crucial for low-loss THz transmission. Finally, microstrip periodic LWAs with GCPW-MSL transitions were fabricated on the polished InP-wafer using contact lithography. The photograph in Fig. 8 shows the fabricated LWAs. As can be seen, the InP substrate shows a visually glazed surface with just a few breakages at the edges which is an indication for a good TCB bonding strength and high-quality CMP process.

## V. EXPERIMENTAL CHARACTERIZATION

In the THz regime, the influence of the conductor surface roughness must be considered because the electric current density peaks near the conductor surface due to the skin effect. For that reason, we measured the surface roughness of the fabricated structure by means of a DektakXT stylus profiler. For a length of 500  $\mu\text{m}$ , altogether 5000 measurement points of the Au surface of the fabricated microstrip LWA were taken. The measured roughness profile is plotted in Fig. 9. As can be seen, the surface height fluctuates only between  $\pm 12$  nm. In order to consider this surface roughness in our simulation model, we calculated the root-mean-square (rms) roughness according to [65]

$$R_q = \sqrt{\frac{1}{n} \sum_{i=1}^n y_i^2} \quad (8)$$

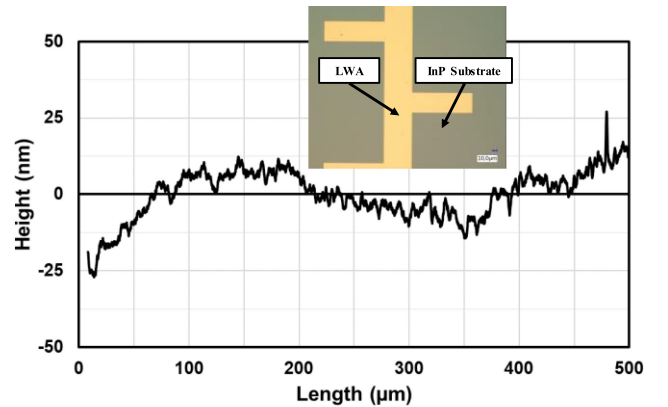


Fig. 9. Measured roughness of microstrip LWA surface by means of a DektakXT stylus profiler. Insert shows a microscopic photo of a fabricated LWA section.

where  $n$  is the number of measured samples and  $y$  is measured height. This results in an rms roughness of  $\sim 8.3$  nm.

The skin depth determines the depth at which the current density is attenuated to  $1/e$  compared to the surface value and it can be calculated using [66]

$$\delta(T) = \frac{c}{\sqrt{2\pi\sigma_0(T)}f} \text{ for } l(T) \ll \delta(T), l(T) \ll \frac{v_F}{f} \quad (9)$$

where  $\sigma_0$  is the static electric conductivity,  $l$  is the mean free path of a conduction electron, and  $v_F$  is the Fermi velocity (for Au at room temperature:  $\sigma_0 = 3 \times 10^{17} \text{ s}^{-1}$  [66],  $l = 37.7$  nm [67], and  $v_F = 13.82 \times 10^5 \text{ m/s}$  [67]). The skin depth for an Au conductor at 300 GHz is 398.9 nm, which indicates that the impact of the surface roughness is not significant.

The simulated  $S_{11}$  of the microstrip periodic LWA with GCPW-MSL transition (black solid line) is shown in Fig. 10. Outside the stopband at 273 GHz, the return loss is lower than 10 dB. Note that the slight change of the broadside frequency is



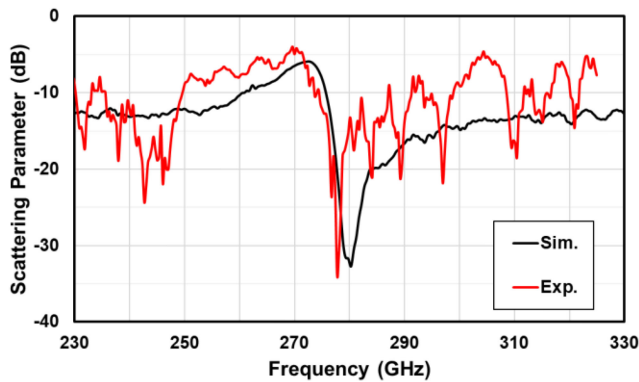


Fig. 10. Simulated and measured  $S_{11}$  parameters of the GCPW-MSL transition with the microstrip periodic LWA.

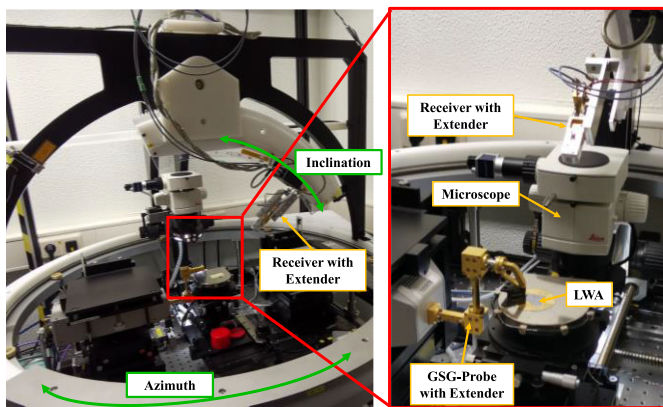


Fig. 11. On-wafer antenna measurement system for far-field radiation pattern measurements.

caused by the transition. For experimental  $S_{11}$  characterization, a VNA (Agilent Technologies 8361A) with a millimeter wave VNA extender (OML V03VNA2-T/R) were used. As can be seen in Fig. 10, the simulation results and the experimentally determined values (red solid line) are in good agreement, which is also an indication for good calibration at such high frequencies.

To experimentally verify beam steering using the fabricated LWA, a THz on-wafer antenna measurement system was developed for measuring the far-field radiation pattern [68]. Here, a VNA (Rohde & Schwarz ZVA-40) and two extenders (Rohde & Schwarz ZC330 and ZRX330), one for signal generation and the other one for signal detection, were used to characterize the beam profile between 220 and 330 GHz. As can be seen from Fig. 11, the receiver has been installed on an automatic hemispherical goniometer system. A C-shaped sliding rail enables receiver movement over an inclination range from  $0^\circ$  to  $51^\circ$ . A  $360^\circ$  rotation in the horizontal plane is carried out by another ring sliding rail. A GSG-probe was used to contact the GCPW-MSL transition of the fabricated LWA for feeding the THz signal. The whole measurement system is placed on an optical table for vibration isolation. It needs to be mentioned that the far-field radiation pattern of the antenna could only be

measured correctly between 273 and 330 GHz. This is because for frequencies lower than 273 GHz, the antenna radiates toward backfire, and the beam is then partially reflected by the GSG-probe.

Fig. 12 shows the simulated and the experimentally determined far-field radiation patterns for different frequencies and for two different antennas. In detail, results are shown for a 1.5-mm wide (a) and an uncleaved (b) InP-based THz LWA. For the measurement, the far-field patterns have been characterized for the same carrier frequencies in steps of  $2^\circ$  over an inclination range from  $0^\circ$  to  $50^\circ$  and in steps of  $5^\circ$  over the full horizontal plane ( $360^\circ$ ).

It can be observed that the radiation patterns of the thinner 1.5-mm wide LWA exhibit a fanlike beam, whereas the radiation patterns of the uncleaved LWA exhibit multiple fingerlike lobes. Note that the “finger-beams” are not grating lobes but are caused by surface wave modes excited in the wide uncleaved InP-to-Si substrate. It is worth mentioning at this point that such “fingerlike” beams can be mitigated by using an array of LWA, which is discussed for THz interconnects in Section VI.

Overall, an excellent agreement between the simulated and the experimentally determined beam patterns is found. The steering angles and even the fingerlike radiation patterns qualitatively agree very well for each frequency. Even the sidelobes for the uncleaved antenna can be clearly observed, which highlights the sensitivity of the developed measurement system. For the 1.5-mm wide antenna, one can observe some stronger sidelobes which are traced back to the impact of the nearby edge which is very rough due to the sawing process.

For a quantitative comparison, the beam direction, 3-dB beam width, and realized gain for the two antennas are shown versus the carrier frequency in Figs. 13–15. These figures also show the expected performances from simulations.

As can be seen from Fig. 13, the simulated beam directions of the designed LWA are not influenced by the width of antenna substrate and sweep from  $-46^\circ$  to  $42^\circ$  by changing the frequency from 230 to 330 GHz, which is successfully confirmed by the corresponding measured results from 280 to 330 GHz. Only around 320 GHz, measured beam angles of the LWA with a 1.5-mm wide substrate are slightly lower than the simulated values due to the rough edges. Fig. 14 shows that the maximum 3-dB beam widths in the H-plane of both LWAs are  $\sim 17^\circ$  at 230 GHz and reduce with increasing frequency. Nonetheless, the minimum value is still larger than  $9^\circ$ . Measurement results confirm the simulated values and demonstrate the impact of edge roughness on the performance of 1.5-mm wide LWA at higher frequencies again. It can be observed from Fig. 15 that the measured average realized gain of the LWA with an uncleaved substrate between 280 and 330 GHz is  $\sim 8.4$  dBi, which is about 4.3 dB lower than the simulated value within this frequency range. The somewhat lower gain of the fabricated antenna can be explained partly by calibration issues and the fact that the pitch of the GSG-probe used for experimental characterization was not perfect for the antenna design. Using a compatible GSG-probe, the LWA with a 1.5-mm wide substrate was measured and the results show a good agreement with simulated values consequently.

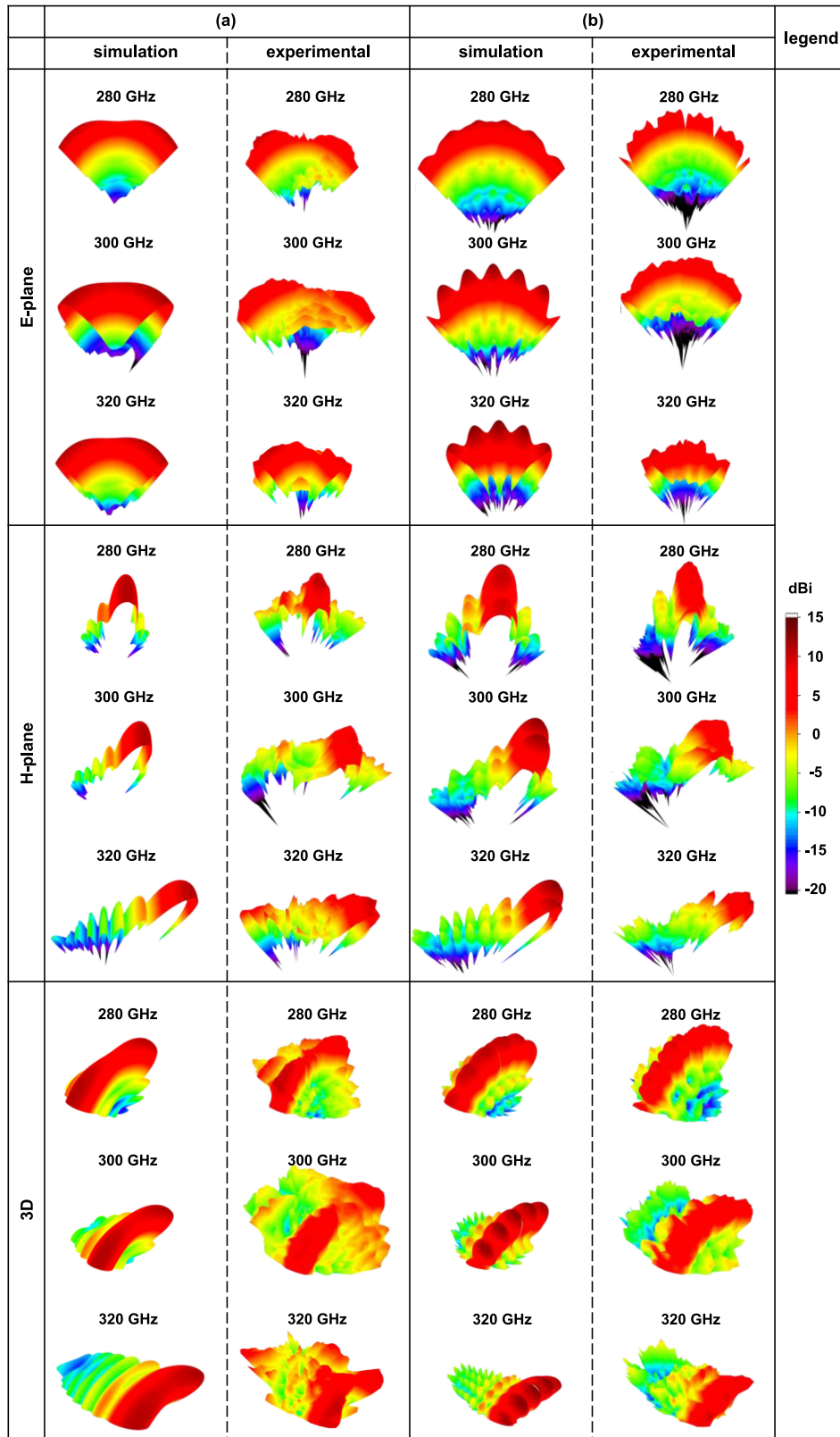


Fig. 12. Simulated and experimentally determined far-field radiation patterns of the microstrip LWA with a GCPW-MSL transition on (a) 1.5 mm wide substrate and (b) uncleaved substrate at 280, 300, and 320 GHz.



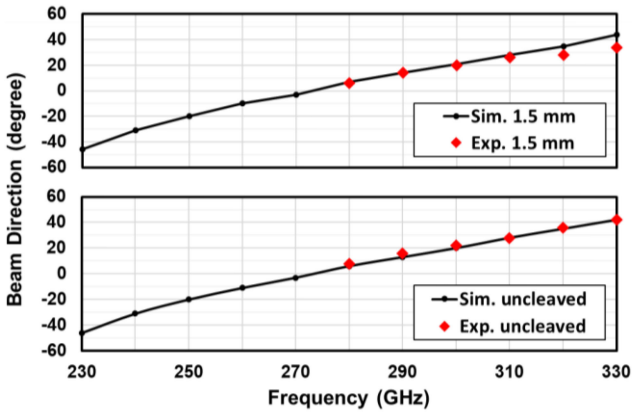


Fig. 13. Simulated and measured relationship between beam direction and frequency from 230 to 330 GHz of the microstrip periodic LWA with GCPW-MSL transition.

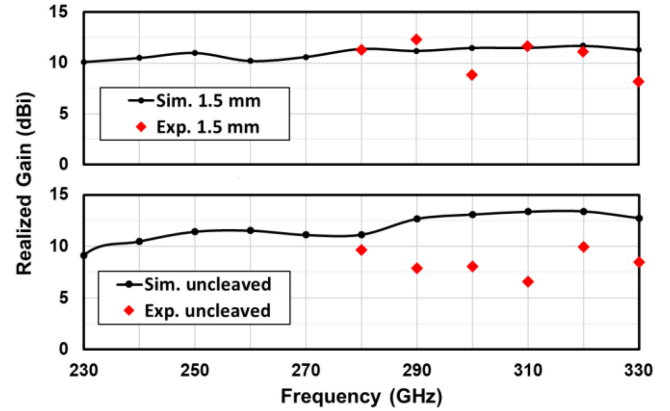


Fig. 15. Simulated and measured relationship between realized gain and frequency from 230 to 330 GHz of the microstrip periodic LWA with GCPW-MSL transition.

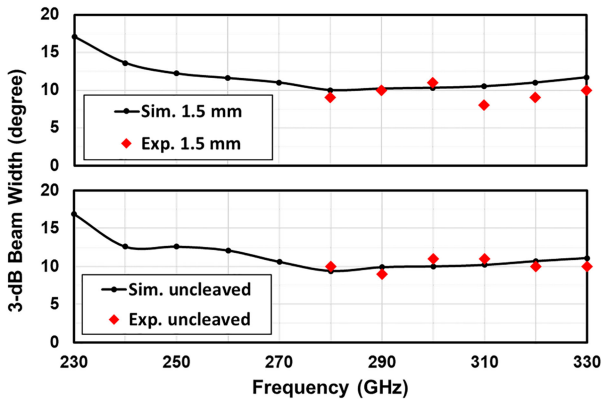


Fig. 14. Simulated and measured relationship between 3-dB beam width and frequency from 230 to 330 GHz of the microstrip periodic LWA with GCPW-MSL transition.

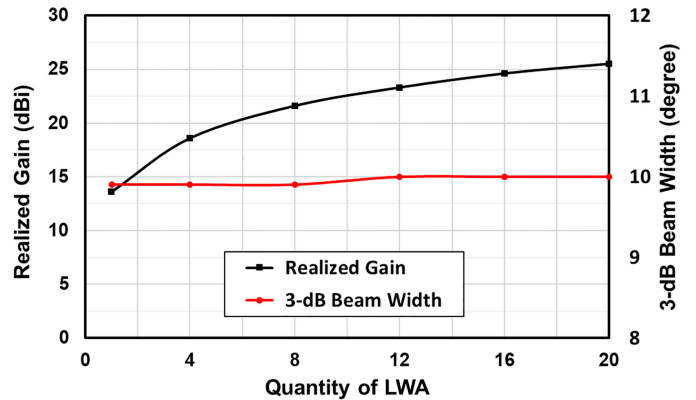


Fig. 16. Simulated realized gain and 3-dB beam width in the H-plane as a function of LWA quantity at 0.3 THz.

## VI. TWO-DIMENSIONAL LWA ARRAY FOR THZ INTERCONNECTS

The InP-based THz beam steering LWA developed in this work yields quasi-linear THz beam steering with  $\sim 0.7^\circ/\text{GHz}$  from 260 to 330 GHz. In this frequency range, the 3-dB beam width in the H-plane is approximately  $10^\circ$ , as shown in Fig. 14. Therefore, the developed LWA could provide a coherence bandwidth exceeding 10 GHz. The transmission distance using a single LWA with an integrated PD is expected to be over 30 cm, as mentioned in Section I. To extend the wireless distance, we suggest using an array of LWAs for THz interconnects. Such an array can now be fabricated in a quite straightforward manner thanks to the possibility of monolithic integration on InP. This would be beneficial in three aspects—it would allow to coherently combine the output power of multiple PDs, it would substantially increase the realized gain of the antenna and it would allow 2-D beam steering. Fig. 16 shows the simulated realized gain and the 3-dB beam width in the H-plane, both at 0.3 THz, as a function of the array size for an LWA array with an antenna pitch of  $500 \mu\text{m}$ . It can be seen that 3-dB beam width in the H-plane is almost constant but the realized gain is

substantially increased, benefiting from a higher directivity in the orthogonal spatial dimension.

For example, when using four parallel LWAs instead of only one, the realized gain at 0.3 THz would increase by about 5 dB and in addition, the output power could be increased by up to 6 dB, when neglecting additional losses at this point. Using Friis equation, we can then estimate that the wireless transmission distance could be extended by a factor of three to around 1 m. This would be sufficient for high data rate THz interconnects between TV sets or inside cabinets used in data centers.

Moreover, it can also be seen from Fig. 17(a) that the far-field radiation pattern for four LWAs on a wide substrate is not “finger-beam” anymore as observed in Fig. 12. Thanks to the array, a focused pencil beam is radiated, i.e., there would be no antenna-related signal distortion.

Finally, 2-D beam steering is achieved when using an additional photonic true time delay which allows to tune the time delay at each of the four photodiodes individually [69]. It can be observed from Fig. 17(b) that with a time delay of 0.5 ps between each LWA, the beam is steered not only in the H-plane, but also in the E-plane with  $\varphi = 318^\circ$  and  $\theta = 28^\circ$ , respectively.

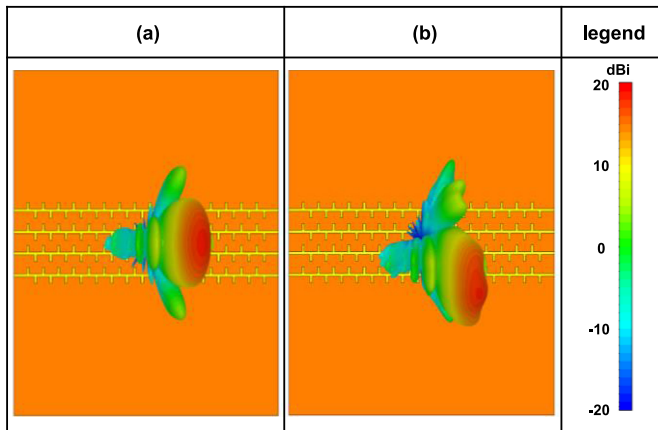


Fig. 17. Simulated far-field radiation pattern of a  $1 \times 4$  microstrip periodic LWA array with a time delay of (a) 0 ps and (b) 0.5 ps between each LWA at 0.3 THz (top view).

In the future and for 2-D steering, the LWA array thus needs to be integrated with an optical beam forming network (OBFN) chip.

## VII. CONCLUSION

This article reports on the design, fabrication, and experimental characterization of an InP-based THz beam steering LWA. To our knowledge, this is the first THz LWA based upon InP substrate, which is an important step toward future monolithic integration with active photonic or electronic THz sources and receivers. The antenna includes a novel grounded coplanar waveguide to microstrip line transition that has been integrated to facilitate future monolithic integration with InP-based THz photodiodes. For being able to fabricate the LWAs on very thin InP, a substrate-transfer process using silicon as carrier substrate has been established. The developed process allows fabrication of the THz structures with an rms roughness of only 8.3 nm. Experimental THz scattering parameter analysis and THz far-field measurements yield a good agreement between the simulated and the experimentally determined antenna performances. Quantitatively, the fabricated THz LWA provides quasi-linear THz beam steering with  $0.7^\circ/\text{GHz}$  from 260 to 330 GHz, i.e., a total steering angle of  $88^\circ$ . For a 1.5-mm wide InP antenna, the achieved 3-dB beam width and realized gain are  $\sim 10^\circ$  and 11 dBi.

Finally, we discussed the use of the developed LWAs for THz interconnects. For an array consisting of four LWAs, a pencil beam with a coherence bandwidth of 10 GHz and a maximum realized gain over 18 dBi is achieved, which is estimated to support wireless THz transmission up to 1 m.

## ACKNOWLEDGMENT

The authors would like to thank R. Zatta and T. Bücher from Bergische Universität Wuppertal, Germany, for the experimental THz  $S_{11}$  scattering parameter measurements, and E. Mutlu from Universität Duisburg-Essen, Germany, for the cleaving of LWAs.

## REFERENCES

- [1] A. Fitzgerald, E. Berry, N. Zinovev, G. Walker, M. Smith, and J. Chamberlain, "An introduction to medical imaging with coherent terahertz frequency radiation," *Phys. Med. Biol.*, vol. 47, no. 7, pp. R67–R84, Mar. 2002.
- [2] C. Yu, S. Fan, Y. Sun, and E. Pickwell-MacPherson, "The potential of terahertz imaging for cancer diagnosis: A review of investigations to date," *Quant. Imag. Med. Surg.*, vol. 2, no. 1, pp. 33–45, Mar. 2012.
- [3] L. Wu *et al.*, "Study of in vivo brain glioma in a mouse model using continuous-wave terahertz reflection imaging," *Biomed. Opt. Express*, vol. 10, no. 8, pp. 3953–3962, Aug. 2019.
- [4] L. Yu *et al.*, "The medical application of terahertz technology in non-invasive detection of cells and tissues: Opportunities and challenges," *RSC Adv.*, vol. 9, no. 17, pp. 9354–9363, Mar. 2019.
- [5] M. Koch, S. Hunsche, P. Schumacher, M. Nuss, J. Feldmann, and J. Fromm, "THz-imaging: A new method for density mapping of wood," *Wood Sci. Technol.*, vol. 32, no. 6, pp. 421–427, Dec. 1998.
- [6] M. Hu *et al.*, "A wavelet-predominant algorithm can evaluate quality of THz security image and identify its usability," *IEEE Trans. Broadcast.*, vol. 66, no. 1, pp. 140–152, Mar. 2010.
- [7] X. Zhang and J. Xu, *Introduction to THz Wave Photonics*. New York, NY, USA: Springer, 2010.
- [8] D. M. Mittleman, "Twenty years of terahertz imaging," *Opt. Express*, vol. 26, no. 8, pp. 9417–9431, Apr. 2018.
- [9] S. Hisatake, J.-Y. Kim, K. Ajito, and T. Nagatsuma, "Self-heterodyne spectrometer using uni-traveling-carrier photodiodes for terahertz-wave generators and optoelectronic mixers," *J. Lightw. Technol.*, vol. 32, no. 20, pp. 3683–3689, Oct. 2014.
- [10] A. Majeed *et al.*, "Broadband THz absorption spectrometer based on excitonic nonlinear optical effects," *Light, Sci. Appl.*, vol. 8, no. 1, pp. 1–5, Mar. 2019.
- [11] J. Y. Suen, M. T. Fang, S. P. Denny, and P. Lubin, "Modeling of terabit geostationary terahertz satellite links from globally dry locations," *IEEE Trans. THz Sci. Technol.*, vol. 5, no. 2, pp. 299–313, Mar. 2015.
- [12] T. Nagatsuma, G. Ducournau, and C. C. Renaud, "Advances in terahertz communications accelerated by photonics," *Nature Photon.*, vol. 10, no. 6, pp. 371–379, Jun. 2016.
- [13] M. F. Hermelo, P.-T. Shih, M. Steeg, A. Ng'oma, and A. Stöhr, "Spectral efficient 64-QAM-OFDM terahertz communication link," *Opt. Express*, vol. 25, no. 16, pp. 19360–19370, Aug. 2017.
- [14] J. W. Holloway, G. C. Dogiamis, and R. Han, "Innovations in terahertz interconnects: High-speed data transport over fully electrical terahertz waveguide links," *IEEE Microw. Mag.*, vol. 21, no. 1, pp. 35–50, Jan. 2020.
- [15] H. Ito and T. Ishibashi, "Photonic terahertz-wave generation using slot-antenna-integrated uni-traveling-carrier photodiodes," *IEEE J. Sel. Topics Quantum Electron.*, vol. 23, no. 4, pp. 1–7, Jul./Aug. 2017.
- [16] K. Ahi, "Review of GaN-based devices for terahertz operation," *Opt. Eng.*, vol. 56, no. 9, pp. 1–14, Sep. 2017.
- [17] R. Lewis, "A review of terahertz detectors," *J. Phys. D, Appl. Phys.*, vol. 52, no. 43, Aug. 2019, Art. no. 433001.
- [18] Y. Monnai, K. Altmann, C. Jansen, H. Hillmer, M. Koch, and H. Shinoda, "Terahertz beam steering and variable focusing using programmable diffraction gratings," *Opt. Express*, vol. 21, no. 2, pp. 2347–2354, Jan. 2013.
- [19] Y. Yang, O. D. Gurbuz, and G. M. Rebeiz, "An eight-element 370–410-GHz phased-array transmitter in 45-nm CMOS SOI with peak EIRP of 8–8.5 dBm," *IEEE Trans. Microw. Theory Techn.*, vol. 64, no. 12, pp. 4241–4249, Dec. 2016.
- [20] X. Li *et al.*, "Switchable multifunctional terahertz metasurfaces employing vanadium dioxide," *Sci. Rep.*, vol. 9, no. 1, pp. 1–13, Apr. 2019.
- [21] M. Tamagnone *et al.*, "Graphene reflectarray metasurface for terahertz beam steering and phase modulation," 2018, *arXiv:1806.02202*.
- [22] T. Nagatsuma, A. Hirata, N. Shimizu, H. Song, and N. Kukutsu, "Photonic generation of millimeter and terahertz waves and its applications," in *Proc. 19th Int. Conf. Appl. Electromagn. Commun.*, Dubrovnik, Croatia, Sep. 2007, pp. 1–4.
- [23] D. Sun *et al.*, "Photonic generation of millimeter and terahertz waves with high phase stability," *Opt. Lett.*, vol. 39, no. 6, pp. 1493–1496, Mar. 2014.
- [24] Y. Zhou, G. Sakano, Y. Yamanaka, H. Ito, T. Ishibashi, and K. Kato, "600-GHz-wave beam steering by terahertz-wave combiner," in *Proc. Opt. Fiber Commun.*, San Diego, CA, USA, Mar. 2018, pp. 1–3.
- [25] K. Maki and C. Otani, "Terahertz beam steering and frequency tuning by using the spatial dispersion of ultrafast laser pulses," *Opt. Express*, vol. 16, no. 14, pp. 10158–10169, Jul. 2008.

- [26] M. Steeg, N. Yonemoto, J. Tebart, and A. Stöhr, "Substrate-integrated waveguide PCB leaky-wave antenna design providing multiple steerable beams in the V-band," *Electronics*, vol. 6, no. 4, Dec. 2017, Art. no. 107.
- [27] P. W. Hon, A. A. Tavallae, Q. Chen, B. S. Williams, and T. Itoh, "Radiation model for terahertz transmission-line metamaterial quantum-cascade lasers," *IEEE Trans. THz Sci. Technol.*, vol. 2, no. 3, pp. 323–332, May 2012.
- [28] K. Murano *et al.*, "Low-profile terahertz radar based on broadband leaky-wave beam steering," *IEEE Trans. THz Sci. Technol.*, vol. 7, no. 1, pp. 60–69, Jan. 2017.
- [29] M. Urteaga, Z. Griffith, M. Seo, J. Hacker, and M. J. Rodwell, "InP HBT technologies for THz integrated circuits," *Proc. IEEE*, vol. 105, no. 6, pp. 1051–1067, Jun. 2017.
- [30] M. Božanić and S. Sinha, "Emerging transistor technologies capable of terahertz amplification: A way to re-engineer terahertz radar sensors," *Sensors*, vol. 19, no. 11, May 2019, Art. no. 2454.
- [31] M. Steeg *et al.*, "Polarization diversity photoreceiver integration on 26 GHz PCB leaky-wave antenna for photonic beam steering transmitter," in *Proc. Int. Topical Meeting Microw. Photon.*, 2019, pp. 1–4.
- [32] A. Pascual *et al.*, "A scalable photomixing array for increased emitted power," in *Proc. 44th Int. Conf. Infrared, Millimeter, Terahertz Waves*, 2019, pp. 1–2.
- [33] A. J. Pascual-Gracia *et al.*, "A photonically-excited leaky-wave antenna array at E-band for 1-D beam steering," *Appl. Sci.*, vol. 10, no. 10, 2020, Art. no. 3474.
- [34] K. M. Leong *et al.*, "A 340–380 GHz integrated CB-CPW-to-waveguide transition for sub millimeter-wave MMIC packaging," *IEEE Microw. Wireless Compon. Lett.*, vol. 19, no. 6, pp. 413–415, Jun. 2009.
- [35] D. Torres *et al.*, "Microcoaxial interconnects for signals, bias, and supply of MMICs," in *Proc. IEEE MTT-S Int. Microw. Symp.*, 2019, pp. 1046–1049.
- [36] K. Neophytou, S. Iezekiel, M. Steeg, and A. Stöhr, "Design of PCB leaky-wave antennas for wide angle beam steering," in *Proc. 11th German Microw. Conf.*, 2018, pp. 152–155.
- [37] S. Dülme *et al.*, "300 GHz photonic self-mixing imaging-system with vertical illuminated triple-transit-region photodiode terahertz emitters," in *Proc. Int. Top. Meeting Microw. Photon.*, Ottawa, ON, Canada, Oct. 2019, pp. 1–4.
- [38] T. Ishibashi, Y. Muramoto, T. Yoshimatsu, and H. Ito, "Unitraveling-carrier photodiodes for terahertz applications," *IEEE J. Sel. Topics Quantum Electron.*, vol. 20, no. 6, pp. 79–88, Nov./Dec. 2014.
- [39] C. A. Balanis, *Modern Antenna Handbook*. Hoboken, NJ, USA: Wiley, 2008.
- [40] J. A. Hejase, P. R. Paladhi, and P. P. Chahal, "Terahertz characterization of dielectric substrates for component design and nondestructive evaluation of packages," *IEEE Trans. Compon., Packag., Manuf. Technol.*, vol. 1, no. 11, pp. 1685–1694, Nov. 2011.
- [41] D. Pozar, "Considerations for millimeter wave printed antennas," *IEEE Trans. Antennas Propag.*, vol. AP-31, no. 5, pp. 740–747, Sep. 1983.
- [42] A. A. Oliner, D. R. Jackson, and J. Volakis, "Leaky-wave antennas," in *Antenna Engineering Handbook*, 4th ed. New York, NY, USA: McGraw-Hill, 2007, ch. 11.
- [43] L. Goldstone and A. Oliner, "Leaky-wave antennas I: Rectangular waveguides," *IRE Trans. Antennas Propag.*, vol. 7, no. 4, pp. 307–319, Oct. 1959.
- [44] P. Lampariello, F. Frezza, H. Shigesawa, M. Tsuji, and A. A. Oliner, "A versatile leaky-wave antenna based on stub-loaded rectangular waveguide. I. Theory," *IEEE Trans. Antennas Propag.*, vol. 46, no. 7, pp. 1032–1041, Jul. 1998.
- [45] J. Liu, D. R. Jackson, and Y. Long, "Substrate integrated waveguide (SIW) leaky-wave antenna with transverse slots," *IEEE Trans. Antennas Propag.*, vol. 60, no. 1, pp. 20–29, Jan. 2012.
- [46] M. Steeg, B. Khani, V. Rymanov, and A. Stöhr, "Novel 50–70 GHz compact PCB leaky-wave antenna with high broadside efficiency and low return loss," in *Proc. 41st Int. Conf. Infrared, Millimeter, Terahertz Waves*, Copenhagen, Denmark, Sep. 2016, pp. 1–2.
- [47] R. Agrawal, P. Belwal, and S. Gupta, "Asymmetric substrate integrated waveguide leaky wave antenna with open stop band suppression and radiation efficiency equalization through broadside," *Radioengineering*, vol. 27, no. 2, pp. 409–416, Jun. 2018.
- [48] A. Grbic and G. V. Eleftheriades, "Leaky CPW-based slot antenna arrays for millimeter-wave applications," *IEEE Trans. Antennas Propag.*, vol. 50, no. 11, pp. 1494–1504, Nov. 2002.
- [49] S. Xiao, B.-Z. Wang, X.-S. Yang, and G. Wang, "A novel reconfiguration CPW leaky-wave antenna for millimeter-wave application," *Int. J. Infrared Millimeter Waves*, vol. 23, no. 11, pp. 1637–1648, Nov. 2002.
- [50] F. Xu and K. Wu, "Understanding leaky-wave structures: A special form of guided-wave structure," *IEEE Microw. Mag.*, vol. 14, no. 5, pp. 87–96, Jul./Aug. 2013.
- [51] P. Baccarelli, P. Burghignoli, F. Frezza, A. Galli, and P. Lampariello, "Novel modal properties and relevant scanning behaviors of phased arrays of microstrip leaky-wave antennas," *IEEE Trans. Antennas Propag.*, vol. 51, no. 12, pp. 3228–3238, Dec. 2003.
- [52] J. James and P. Hall, "Microstrip antennas and arrays. Part 2: New array-design technique," *IEE J. Microw., Opt. Acoust.*, vol. 1, no. 5, pp. 175–181, Sep. 1977.
- [53] S. Bedair and M. Sobhy, "Accurate formulas for computer-aided design of shielded microstrip circuits," *IEE Proc. H - Microw., Opt. Antennas*, vol. 127, no. 6, pp. 305–308, Dec. 1980.
- [54] D. H. Schrauder, *Microstrip Circuit Analysis*. Upper Saddle River, NJ, USA: Prentice Hall, 1995.
- [55] D. M. Pozar, *Microwave Engineering*, 3rd ed. Hoboken, NJ, USA: Wiley, 2005.
- [56] P. Baccarelli, S. Paulotto, D. R. Jackson, and A. A. Oliner, "A new Brillouin dispersion diagram for 1-D periodic printed structures," *IEEE Trans. Microw. Theory Techn.*, vol. 55, no. 7, pp. 1484–1495, Jul. 2007.
- [57] B. Xi *et al.*, "Periodic fixed-frequency staggered line leaky wave antenna with wide-range beam scanning capacity," *IEEE Access*, vol. 7, pp. 146693–146701, 2019.
- [58] S. Paulotto, P. Baccarelli, F. Frezza, and D. R. Jackson, "A novel technique for open-stopband suppression in 1-D periodic printed leaky-wave antennas," *IEEE Trans. Antennas Propag.*, vol. 57, no. 7, pp. 1894–1906, Jul. 2009.
- [59] G. Zheng, J. Papapolymerou, and M. M. Tentzeris, "Wideband coplanar waveguide RF probe pad to microstrip transitions without via holes," *IEEE Microw. Wireless Compon. Lett.*, vol. 13, no. 12, pp. 544–546, Dec. 2003.
- [60] A. Chahadhi, P. Y. Cresson, C. Mismar, and T. Lasri, "V-band via-less GCPW-to-microstrip transition designed on PET flexible substrate using inkjet printing technology," *IEEE Microw. Wireless Compon. Lett.*, vol. 25, no. 7, pp. 436–438, Jul. 2015.
- [61] M. El-Gibari *et al.*, "Ultra-broad bandwidth and low-loss GCPW-MS transitions on low-k substrates," *Electron. Lett.*, vol. 46, no. 13, pp. 931–933, 2010.
- [62] J.-P. Raskin, G. Gauthier, L. P. Katehi, and G. M. Rebeiz, "Mode conversion at GCPW-to-microstrip-line transitions," *IEEE Trans. Microw. Theory Techn.*, vol. 48, no. 1, pp. 158–161, Jan. 2000.
- [63] R. Simons, *Coplanar Waveguide Circuits, Components, and Systems*. New York, NY, USA: Wiley, 2001.
- [64] A. W. Fang *et al.*, "Hybrid silicon evanescent devices," *Mater. Today*, vol. 10, no. 7/8, pp. 28–35, Jul./Aug. 2007.
- [65] E. Gadelmawla, M. Koura, T. Maksoud, I. Elewa, and H. Soliman, "Roughness parameters," *J. Mater. Process. Technol.*, vol. 123, no. 1, pp. 133–145, Apr. 2002.
- [66] V. Bezerra, G. Bimonte, G. Klimchitskaya, V. Mostepanenko, and C. Romero, "Thermal correction to the Casimir force, radiative heat transfer, and an experiment," *Eur. Phys. J. C*, vol. 52, no. 3, pp. 701–720, 2007.
- [67] D. Gall, "Electron mean free path in elemental metals," *J. Appl. Phys.*, vol. 119, no. 8, 2016, Art. no. 085101.
- [68] B. Sievert, J. T. Svejda, D. Erni, and A. Rennings, "Spherical mm-wave/THz antenna measurement system," *IEEE Access*, vol. 8, pp. 89680–89691, 2020.
- [69] M. Steeg, P. Lu, J. Tebart, and A. Stöhr, "2D mm-wave beam steering via optical true-time delay and leaky-wave antennas," in *Proc. 12th German Microw. Conf.*, Stuttgart, Germany, Mar. 2019, pp. 158–161.



**Peng Lu** was born in Tianjin, China. He received the B.Sc. and M.Sc. degrees in nanoengineering/nano-optoelectronics from the University of Duisburg-Essen, Duisburg, Germany, in 2014 and 2016, respectively.

Since 2017, he has been a Member of the Department of Optoelectronics, Center for Semiconductor Technology and Optoelectronics (ZHO), and a Research Associate with the University of Duisburg-Essen. His current research interests include photonic integrated chips (PICs) for terahertz

beam forming, terahertz leaky-wave antenna, and 3-D hybrid integration of III-V-Si platforms.





**Thomas Haddad** (Graduate Student Member, IEEE) received the M.Sc. degree in embedded systems from the University of Duisburg-Essen, Duisburg, Germany, in 2019. His master's thesis focused on developing THz leaky wave antennas for beam steering. He is currently working toward the Ph.D. degree with the Optoelectronic Department, University of Duisburg-Essen.

His research interests include technologies of THz beam steering antennas and THz communications and applications.



**Benedikt Sievert** was born in Krefeld, Germany. He received the B.Sc. and M.Sc. degrees in electrical engineering/high frequency systems from the University of Duisburg-Essen, Duisburg, Germany, in 2017 and 2019, respectively.

Since 2017, he has been a Member of the Department of General and Theoretical Electrical Engineering, University of Duisburg-Essen. His current research interests include mm-wave on-chip antennas, electromagnetic metamaterials, and computational electromagnetics.



**Beshar Khani** received the M.Sc. degree in computer science and communications engineering from the University of Duisburg-Essen, Duisburg, Germany, in 2013.

After his study, he has gained international experience with the Department of Electronics Technology, Charles III University of Madrid, Madrid, Spain, within the Marie Curie "MITEPHO" (Microwave and TERAHERTZ PHOTONICS), focusing on the design of novel millimeter-wave circuits using the finite element method high frequency structural simulator

(HFSS). From 2014 to 2019, he was a Member of the Optoelectronics Department, University of Duisburg-Essen. His research includes III/V and RF photonic integration technologies based on high-frequency laminates. He has authored or coauthored more than 30 papers in refereed journals and conferences. His current research interests include the design and development of compact millimeter-wave and THz coherent photonic transmitters and receivers' modules for the 5G mobile communications and photonic radar applications.



**Sumer Makhlof** received the M.Sc. degree in communications engineering from the University of Duisburg-Essen, Duisburg, Germany, in 2018. His master's thesis concentrated on the 3-D printed THz photodiode packages with rectangular waveguide output. He is currently working toward the Ph.D. degree on electronic-phonic integration circuits (EPIC) for THz applications.

He is currently a Member of the Optoelectronics Department, Center for Semiconductor Technology and Optoelectronics (ZHO), and a Research Associate with the University of Duisburg-Essen.



**Sebastian Dülme** was born in Hattingen, Germany. He received the B.Sc. and M.Sc. degrees in nanoengineering/nano-optoelectronics in 2015 and 2017, respectively, from the University of Duisburg-Essen, Duisburg, Germany, where he has been working toward the Ph.D. degree with the Institute of Optoelectronics, since 2017.

His research interests include terahertz photodiodes, terahertz power combining, and terahertz spectroscopy and imaging systems.



**José Fernández Estévez** received education as a microtechnologist of semiconductor technology in 2000.

He is currently a Member of the Optoelectronics Department, Center for Semiconductor Technology and Optoelectronics (ZHO), and Technical Assistant with the University of Duisburg-Essen, Duisburg, Germany.



**Andreas Rennings** (Member, IEEE) studied electrical engineering with the University of Duisburg-Essen, Duisburg, Germany. He carried out his Diploma work with the University of California in Los Angeles, Los Angeles, CA, USA. He received the Dipl.-Ing. and Dr.-Ing. degrees from the University of Duisburg-Essen in 2000 and 2008, respectively.

From 2006 to 2008, he was an RF Engineer with IMST GmbH, Kamp-Lintfort, Germany. Since then, he has been a Senior Scientist and Principal Investigator with the Laboratory for General and Theoretical

Electrical Engineering, University of Duisburg-Essen. His general research interests include all aspects of theoretical and applied electromagnetics, currently with a focus on medical applications and on-chip millimeter-wave/THz antennas.

Dr. Rennings was the recipient of several awards, including a Student Paper Prize at the 2005 IEEE Antennas and Propagation Society International Symposium and the VDE-Promotionspreis 2009 for the dissertation.



**Daniel Erni** (Member, IEEE) received the Diploma from the University of Applied Sciences in Rapperswil (HSR), Rapperswil-Jona, Switzerland, in 1986, the Diploma from ETH Zürich, Zurich, Switzerland, in 1990, both in electrical engineering, and the Ph.D. degree in laser physics from the Laboratory for Electromagnetic Fields and Microwave Electronics, ETH Zürich, in 1996.

Since 1990, he has been with the Laboratory for Electromagnetic Fields and Microwave Electronics, ETH Zürich. From 1995 to 2006, he has been the

Founder and Head of the Communication Photonics Group, ETH Zürich. Since October 2006, he has been a Full Professor of General and Theoretical Electrical Engineering with the University of Duisburg-Essen, Duisburg, Germany. He is a Co-Founder of the spin-off company *airCode* on flexible printed RFID technology. His current research interests include optical interconnects, nanophotonics, plasmonics, advanced solar cell concepts, optical and electromagnetic metamaterials, RF, mm-wave and THz engineering, biomedical engineering, bioelectromagnetics, marine electromagnetics, computational electromagnetics, multiscale and multiphysics modeling, numerical structural optimization, and science and technology studies (STS).

Prof. Erni is a Fellow of the Electromagnetics Academy, a Member of the Center for Nanointegration Duisburg-Essen (CeNIDE), as well as a Member of the Swiss Physical Society (SPS), German Physical Society (DPG), and the Optical Society of America (OSA).





**Ullrich Pfeiffer** (Fellow, IEEE) received the Diploma and Ph.D. degree from the University of Heidelberg, Heidelberg, Germany, in 1996 and 1999, respectively, both in physics.

In 1997, he was a Research Fellow with the Rutherford Appleton Laboratory, Oxfordshire, U.K. From 1999 to 2001, he was a Postdoctoral Researcher with the University of Heidelberg on real-time electronics for particle physics experiments at the European Organization for Nuclear Research (CERN), Meyrin, Switzerland. From 2001 to 2006, he was with the

IBM T.J. Watson Research Center, where his research involved RF circuit design, power amplifier design at 60 and 77 GHz, high-frequency modeling, and packaging for millimeter-wave communication systems. Since 2008, he has been the High-frequency and Communication Technology Chair with the University of Wuppertal, Wuppertal, Germany. In 2007, he led the THz Electronics Group, Institute of High-Frequency and Quantum Electronics, University of Siegen, Siegen, Germany. His current research interests include silicon RFICs for mmWave/THz communication, radar, and imaging systems.

Prof. Pfeiffer was the co-recipient of the 2004 and 2006 Lewis Winner Award for Outstanding Paper at the IEEE International Solid-State Circuit Conference, the co-recipient of the 2006 IBM Pat Goldberg Memorial Best Paper Award, the 2007 European Young Investigator Award, the 2008 EuMIC Best Paper Award, the 2010 EuMC Microwave Prize, the 2014 EuCAP Best Paper Award, and the 2017 Microwave Prize, the 2012 and 2018 Jan Van Vessel Award for Outstanding European Paper at the IEEE International Solid-State Circuit Conference. He has been a Distinguished Lecturer for the IEEE Solid-State Circuits Society and the President of the German Association for Electrical Engineering and Information Technology e.V. (FTEI).



**Andreas Stöhr** (Senior Member, IEEE) received the Dipl.-Ing. and Dr.-Ing. degrees in electrical engineering from Gerhard-Mercator-University, Duisburg, Germany, in 1991 and 1997, respectively.

From 1987 to 1996, he was the CEO of MS Steuerungsanlagen GmbH, Germany. From 1996 to 2013, he was a Research Scientist with the University of Duisburg, Duisburg, Germany. During that period, in 1998 and 1999, he also joined the Communications Research Laboratory (CRL), Tokyo, Japan, where he worked on 60 GHz wireless systems employing radio over fiber techniques. He was also with France Telecom Orange Labs, Lannion, France, in 2009 and with Corning in 2015. He is currently also a Visiting Professor with the University of Ottawa, Ottawa, ON, Canada. Since 2011, he has been a Professor and the Head of the Optoelectronics Department, Center for Semiconductor Technology and Optoelectronics (ZHO), University of Duisburg-Essen (UDE), Duisburg, Germany. He has authored or coauthored more than 200 papers in refereed journals and conferences. His current research interests include III/V integrated microwave photonic device technology and RF photonic integration technologies for millimeter-wave and THz communications, measurement systems, as well as sensing applications.

Prof. Stöhr is a Senior Member of the IEEE Photonics and MTT Society, Committee Member and Chair of a number of international conferences, and IEEE/OSA Guest Editor.